JOURNAL OF MATERIALS SCIENCE 28 (1993) 1334 – 1340

Synthesis of Si(N,C) nanostructured powders from an organometallic aerosol using a hot-wall reactor

T. D. XIAO, K. E. GONSALVES, P. R. STRUTT*, P. G. KLEMENS‡
*Polymer Science Program and Department of Chemistry, and *Department of Metallurgy, Institute of Materials Science, and ‡Department of Physics, University of Connecticut, Storrs, CT 06268, USA*

Current studies show that nanostructured Si(N,C) powders are readily synthesized by rapid condensation of a pyrolytically decomposed silazane precursor, namely $[CH_3SiHNH]_n$, $n=3$ or 4. Basically, the process involves ultrasonic conversion of the liquid-phase precursor to an aerosol, followed by thermal decomposition in a hot reactor. This was followed by the rapid condensation of the gaseous product exiting the reactor, to form ceramic particles of nanoscale dimension. Thermal decomposition was performed at a temperature of 1000 °C, near ambient pressure with a flow rate of ~150 standard $cm^3 min^{-1}$ for NH_3. One critical feature examined in this process was the rapidity of the powder synthesis, in a reaction which involves (i) elimination of ligand groups, (ii) formation of ceramic species, and (iii) condensation of ceramic species into ultrafine ceramic particles. These features have been studied using Fourier transform infrared spectroscopy, transmission electron microscopy, X-ray photo-electron and nuclear magnetic resonance spectroscopies. Additionally, a model is formulated to determine the effect of process parameters on particle size.

1. Introduction

The ability to assemble molecular groups and clusters in a precise and predetermined way opens up interesting possibilities for creating materials possessing highly homogeneous structures, which exhibit improved, and even novel properties. The importance of this concept, in the synthesis of metallic and ceramic materials, has been clearly recognized by Birringer and Gleiter [1], who created what they termed nanocrystalline solids. Structurally these consist of ultrafine grains, with a mean diameter of a few nanometers. Birringer and Gleiter [1], and later Eastman and Siegel [2] produced nanocrystalline materials in the form of powders by rapid vapour-phase condensation of atomic species from simple evaporation sources. Consolidation into bulk samples was achieved by high-pressure compaction.

Currently, nanostructured material synthesis is being addressed, primarily, by the use of physical methods. Because these, however, are inherently slow, methodologies are required for the production of material in large-scale amounts. Such a methodology shown to be viable [3–5] exploits organometallic/-polymer chemistry and materials processing concepts. Metal-organic/polymeric precursors are particularly attractive [6, 7] because they can be used to (i) yield a high fraction of end product, and (ii) obtain phases with a selected stoichiometry. Consequently, this facilitates the production of nanocomposite materials in significant amounts that may contain a diverse range of phases, such as intermetallic, silicide, boride, nitride, carbide and oxide phases.

Previously, a technique was reported [4, 5] for the ultra-rapid conversion of a silazane "monomeric" precursor to an intermediate polymeric preceramic Si–N–C material, in the form of a nanostructured powder. This was accomplished by laser-induced polycondensation and rapid cross-linking, using a method where the liquid precursor was ultrasonically injected into a high-power CO_2 laser beam. The strong energy coupling between the laser radiation and the precursor aerosol resulted in the formation of a plume. Rapid condensation and cross-linking from the plume, together with the strong cross-linking, produced nanostructured particles of a preceramic Si(C,N) phase.

This paper describes an alternative approach to the laser-processing method, in that nanostructured powders are produced by injection of a precursor aerosol into a hot-wall reactor. Particle formation is achieved by rapid condensation of the vapour phase exiting the reactor. Based upon initial results, the method is particularly promising because significant amounts of powder are formed in a relatively short time.

2. Experimental procedure

2.1. Precursor synthesis and properties

The organosilazane precursor was prepared by ammonolysis of methyldichlorosilane according to the

0022–2461

method of Seyferth and Wiseman, [7]. Experimentally, diethyl ether and methyldichlorosilane were cannulated into a flask cooled to 0 °C in an ice bath. An excess of anhydrous ammonia was bubbled into the flask with vigorous stirring until the solution was strongly basic. The reaction mixture was stirred for another 2 h and then filtered under argon. The solvent was removed by trap-to-trap distillation under vacuum, leaving an oily residue. The ammonolysis process yielded a product of mainly cyclics $[CH_3SiHNH]_n$, with $n = 3$ or 4, as well as some linear structures. The major component had $n = 4$ cyclics.

The structure of the liquid silazane precursor is shown in Fig. 1. The molecular weight determined by cryoscopy in benzene was about 290 g mol^{-1}. The boiling point was about 100 °C at 0.01 mm Hg. Thermogravimetric analysis (TGA) of this precursor revealed a progressive weight loss in the 40–450 °C temperature range as shown in Fig. 2. At 450 °C, the cumulative weight loss was 95% with no further loss beyond this temperature. This suggested that direct conversion of the liquid silazane precursor into ceramic product is impossible because this only resulted in the distillation of the cyclic species out of the hot furnace. This phenomenon was also observed by Seyferth and Wiseman [7].

2.2. Processing procedure

The experimental arrangement for the thermal decomposition used to synthesize nanostructured Si(N,C) particles is schematically shown in Fig. 3.

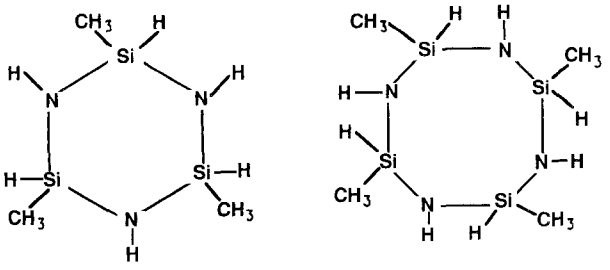

Figure 1 Molecular structure of the organosilazane precursor, $[CH_3SiHNH]_n$, $n = 3$ or 4.

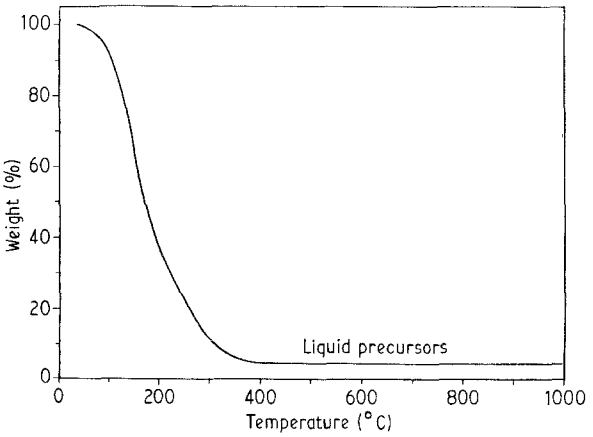

Figure 2 Thermogravimetric analysis of the liquid precursor. Sample size 43.31 mg, scan rate 5 °C min^{-1}.

It consisted of basically three major components: a Sono-Tek ultrasonic atomizer, a hot-wall reactor, and a cooled powder collector. The procedure first involved filling the ultrasonic atomizer supply chamber with the liquid precursor. Following this step, the hot-wall reactor was evacuated to $\sim 10^{-5}$ torr (1 torr = 133.322 Pa) using a diffusion pump, flushed several times with nitrogen gas, and then backfilled with nitrogen to near ambient pressure. The system was maintained with a flow rate of 150 standard cm^3 min^{-1} for NH_3 with a MKS gas flow controller.

During the process operation, the furnace was maintained at a temperature of 1000 °C. The liquid precursor was forced into the ultrasonic nozzle by having a slight negative pressure at the processing chamber. The magnitude of this controlled pressure differential determined the precursor delivery rate. In this study, this was $\sim 9 \times 10^{-3}$ cm^{-3} s^{-1}. The liquid aerosols had an initial velocity of ~ 33 cm s^{-1} at the

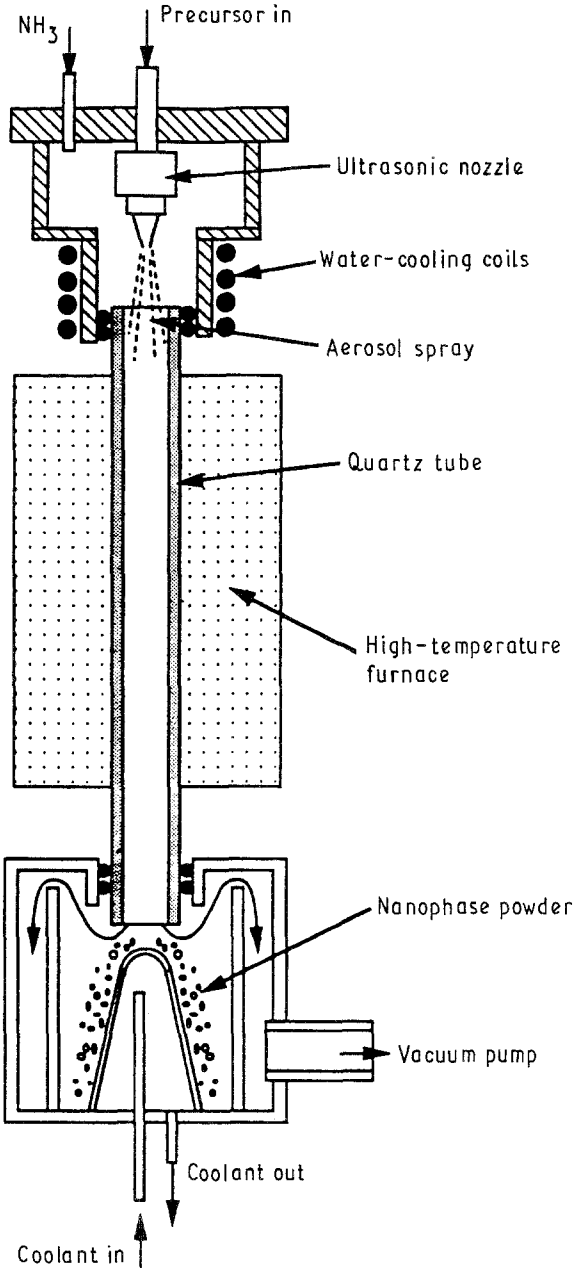

Figure 3 Schematic diagram of the thermal conversion processing system.

nozzle exit. Once they reached the hot reaction zone, they rapidly evaporated into molecular species. During the reaction time, a white smoking stream was observed at the bottom of the reactor exit. Because no visible particle deposition was observed at the hot furnace region, it was assumed that the hot molecules emerging from the reaction zone formed small particles which were then collected at the bottom of the cooled collector.

3. Results and discussion

The silazane precursor has a high degree of reactivity in the Si–H and N–H functionalities, which is a key feature in its rapid cross-linking to form a higher molecular weight preceramic polymer during processing [4, 5]. This preceramic polymer would then form Si_3N_4/SiC ceramics under heat treatment [7]. In the thermal aerosol injection process, silazane aerosols were rapidly evaporated. Reaction of this vapour in the presence of NH_3 resulted in the formation of ceramic molecules in the vapour phase. These ceramic species were then rapidly quenched to form nanoscale ceramic particles near the cooled collector as they emerged from the hot reaction zone [4, 5].

Rapid condensation of the ceramic vapours from the hot reaction zone is intriguing, because this resulted in the formation of ceramic particles with a particle size ~ 60 nm. This rapid condensation process leading to the formation of nanostructured particles does not occur via a conventional chemical process. As mentioned earlier, the TGA data (Fig. 2) revealed a cumulative weight loss of 95% which suggested that direct thermal heating alone could not convert the liquid precursor into ceramic product, because it resulted mainly in the distillation of cyclic species out from the hot furnace. Careful removal of the powder from the cooled collector, when the thermal aerosol decomposition method was used in this study, showed that the liquid to ceramic conversion yield was $\sim 70\%$, and a production rate of approximately 1 g min^{-1} was achieved.

A wide variety of characterization techniques have been used which provided a broad range of compositional and structural information. Detailed microstructural analysis using transmission electron microscopy (TEM) indicated particles are spherical in shape and amorphous. Structural analysis using Fourier transform infrared spectroscopy (FTIR) revealed the elimination of ligand groups with the evidence of Si_3N_4. X-ray photoelectron spectroscopy (XPS) studies provided the chemical composition together with information on the nature of the chemical bonding for the nanostructured ceramic particles. Solid state nuclear magnetic resonance (NMR) gave structural information on the nanostructured particles similar to the XPS analysis.

3.1. Microstructural analysis

The morphological characteristics of the powders were examined by X-ray and transmission electron microscopy (TEM). X-ray analysis using a powder diffractometer indicated no crystalline feature of the ceramic powders. The transmission electron micrographs were obtained using a solution technique, in which powders were dispersed in deoxygenated methanol using an ultrasonic vibrator. These particles were then transferred onto a TEM grid, 200 mesh size coated with a Pt–C film, by dipping it into the above solution. Fig. 4 is representative of the micrographs for the nanoscale ceramic particles. This micrograph showed the transparency of the individual particles and the dark contrast arising from particle overlapping. Electron diffraction revealed these particles to be entirely amorphous. Similar results were also obtained in the TEM studies when the silazane precursor aerosols were pyrolysed using a continuous wave CO_2 laser [4, 5].

3.2. Analysis of structures and composition

Comparative studies of the original liquid precursor and the synthetic nanostructured ceramic particles were performed using Fourier transform infrared spectroscopy (FTIR). In the FTIR studies the liquid precursor was placed inside an NaCl cell and analysed in the transmission mode. Careful examination (Fig. 5a) revealed the following bonds were present in the liquid precursor: N–H at 3380 cm^{-1}, C–H at 2960 cm^{-1}, Si–H at 2150 cm^{-1}, and Si–CH_3 at 1260 cm^{-1}, N–H at 1180 cm^{-1}, and Si–N at 950 and 850 cm^{-1}.

The FTIR studies for the synthesized ceramic particles were carried out using KBr pellets in transmission mode. As shown by Fig. 5b, the ligand groups were eliminated after the thermal decomposition reaction. The FTIR spectra revealed only two broad peaks: a peak at a wave number of about 950 cm^{-1}, and a small peak at 3380 cm^{-1}. The peak at 3380 cm^{-1} could be due to the presence of N–H bonds in the ceramic powders [7]. The peak at 950 cm^{-1} could be due to the Si_3N_4 species [5, 8]. Similar results were also obtained by other investigators when Si_3N_4 was synthesized using plasma enhanced chemical vapour deposition [9], and the N–H peak was often

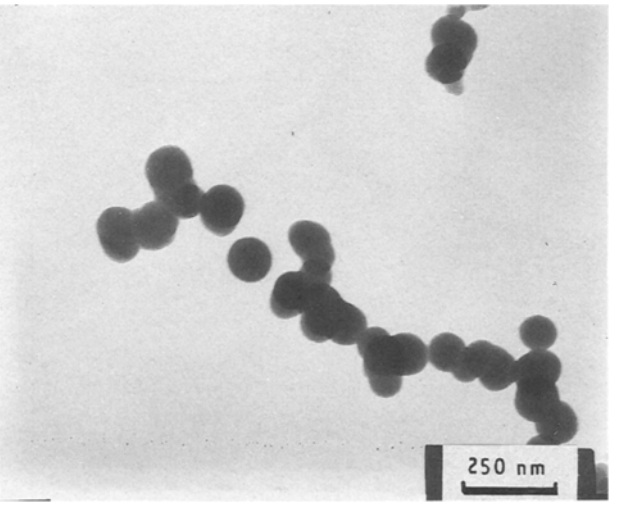

Figure 4 Transmission electron micrograph showing ultrafine ceramic particles derived from pyrolysis of the silazane precursor.

present when the synthesis was performed in an NH_3 environment. An important feature in the FTIR data was the displacement of the peak for the absorption maxima of Si_3N_4, due to the presence of oxygen impurities and an SiC bond [7]. As pointed out by Wong [10], oxygen contamination can cause the Si_3N_4 peak shift to higher wave numbers. The synthesis temperatures can also effect the precise position (860 cm^{-1}) of the Si–N absorption in the amorphous Si_3N_4 [11].

Chemical composition and bonding information were obtained using X-ray photo-electron spectroscopy (XPS). In the XPS studies, ceramic powder was compacted into a pellet using a hydrostatic press. The sample surface was then fractured (or partially removed) to eliminate surface contaminations from the die. The survey spectra (Fig. 6) of the ceramic powder consisted of silicon, nitrogen, carbon and oxygen with a composition of 33.8%, 32.5%, 21.1%, and 12.6%, respectively. A similar chemical composition was also obtained when using the chemical method (chemical analysis was performed by Mikroanalytisches Labor Pascher, Remagen, Germany). Detailed energy values corresponding to various chemical bonds were derived from the XPS spectra recorded in the high-resolution mode.

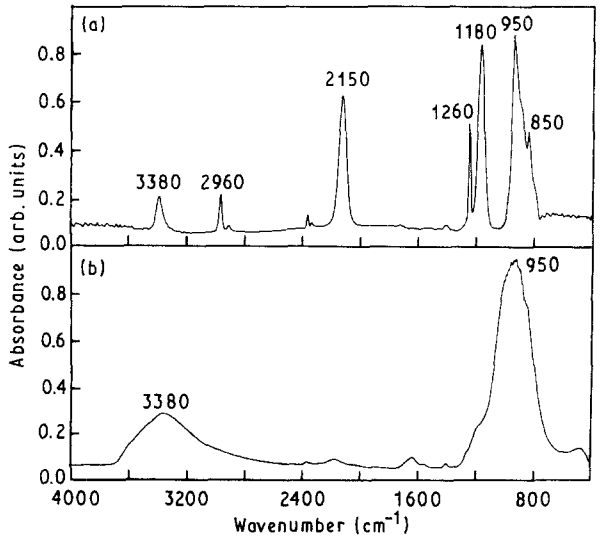

Figure 5 Fourier transform infrared spectrum: (a) liquid precursor, (b) ultrafine ceramic particles derived from the precursor.

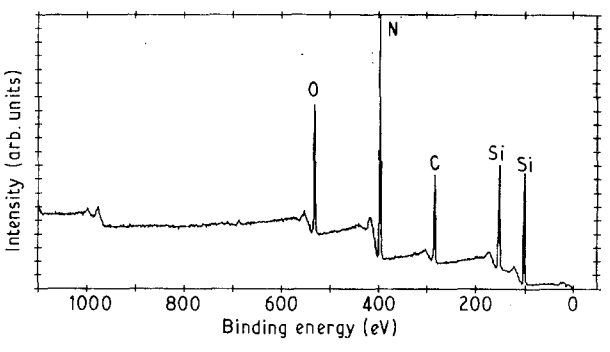

Figure 6 X-ray photoelectron survey spectra of the ultrafine ceramic particles.

3.2.1. Si(2p) region

The Si(2p) spectra consisted of five components. A representative of the curve-fitted spectra is shown in Fig. 7a. Stoichiometric Si_3N_4 would have a binding energy at about 101.4–101.7 eV [12]. According to Karcher, *et al.*, Si–N bond has the tendency to decrease its binding energy for non-stoichiometric Si_xN_y [13], typically 100.2 eV for $SiN_{1.1}$. This energy shift is due to the decreased Si–N bonds that are replaced by Si–Si bonds. Raider *et al.* pointed out that silicon oxynitride would produce a peak between 101.7 and 103.0 eV [12]. Therefore, we assigned Peak 1 at about 100.05 eV to the SiC bond [14], Peak 2 at about 100.8 eV to the nonstoichiometric Si_xN_y bond [13], Peak 3 at about 101.6 eV to the Si_3N_4 bond, Peak 4 at about 102.5 eV to the Si(N,O) bond, and Peak 5 at about 103.4 eV to the SiO_2 bond [12].

3.2.2. C(1s) region

The C(1s) peak consisted of four components (Fig. 7b). Bouillon *et al.* [14], pointed out that the Si–C bond would have a peak around 283–284.2 eV for Si_x–C to Si–C_y, Thus, Peak 1 at about 283.1 eV and peak 2 at about 283.9 eV were assigned to the SiC bond. Peak 3 at about 285.5 eV was assigned to the C–O bond, and Peak 4 at about 287.8 eV to the C=N bond [15]. It should be noted that the C=N bond consisted of about 3.5% of the carbon peak area, which corresponded to about 0.7% of the total composition. The C–O–C bond consisted of about 5.6% of the carbon peak area, which in turn corresponded to 1.2% of the total composition.

3.2.3. N(1s) region

The N(1s) spectra consisted of three peaks (Fig. 7c). Peak 2 at about 397.4 eV was assigned to Si_3N_4 species. Peak 1, at about 396.5 eV, was assigned to the Si_xN_y bond, and Peak 3 at about 398.9 eV was assigned to the Si(N,O) bond. Xie and Scherwood [15], had pointed out that a binding energy near 398 eV could be due to the presence of carbon-bonded nitrogen species.

3.2.4. O(1s) region

The O(1s) spectra was fitted with three peaks (Fig. 7d). Silicon dioxide would have a binding energy near 533.0 eV. According to Xie and Scherwood [15], C–O–C bonds have a binding energy around 531.8 eV Thus, we assigned Peak 1 at about 529.5 eV to the Si(N,O) bond, Peak 2 at about 531.2 eV to carbon-bonded oxygen species, and Peak 3 at about 533.4 eV to the SiO_2 bond. The SiO_2 bond had about 9.2% of the oxygen peak area which corresponded to about 1.2% of the total composition.

Chemical bonding information for the nanostructured ceramic particles was also obtained using magic angle spinning (MAS) solid state nuclear magnetic resonance (NMR) spectroscopy. Resonance peaks were obtained for ^{29}Si and ^{13}C. The ^{29}Si NMR data for the ceramic powders are shown in Fig. 8. Three

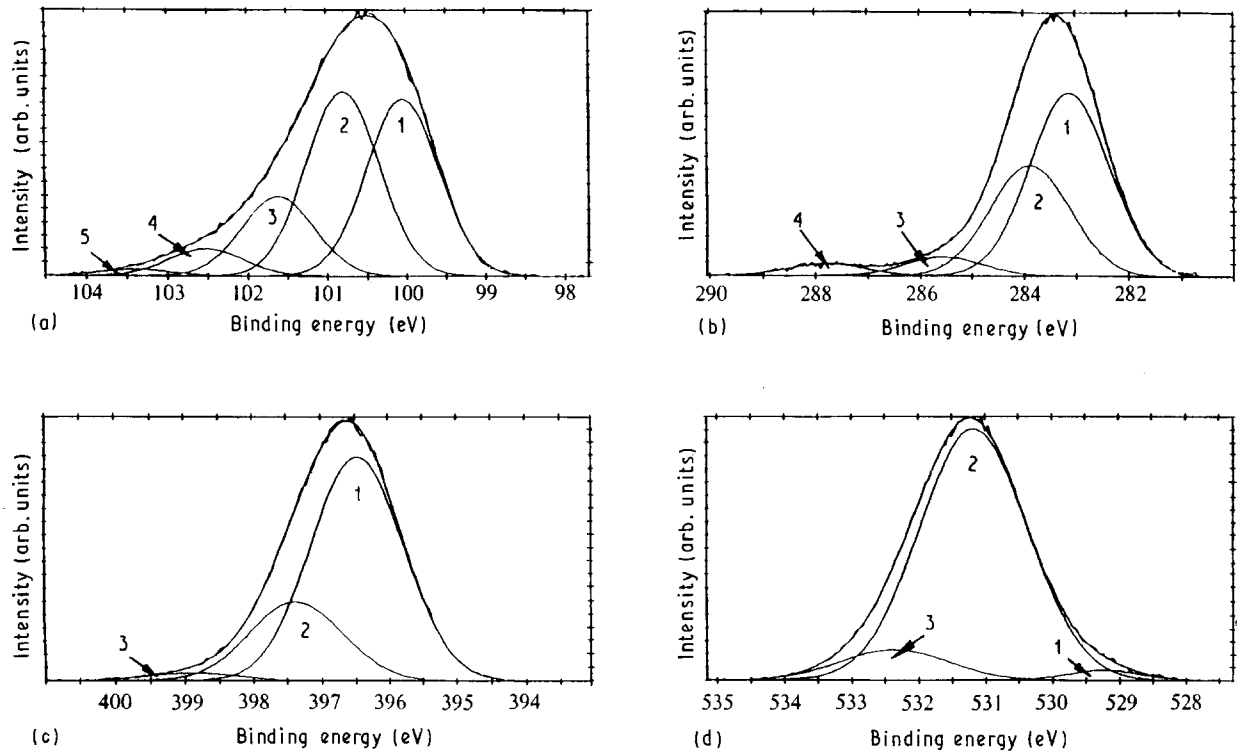

Figure 7 Representative curve-fitted X-ray photo electron spectra showing the chemical bonding characteristics of the ultrafine ceramic particles. (a) Si(2p), (b) C(1s), (c) N(1s), (d) O(1s).

main resonance peaks were observed, centred at approximately -27.4, -43.9 and -98.3 p.p.m., assigned to SiC [16–18], Si_3N_4[17,19,20] and SiO_2[19], respectively. The peak observed at -27.4 p.p.m. could be also due to the silicon unit both bonded with nitrogen and carbon atoms as first neighbours. As pointed out by Babonneau [18], a chemical shift at around -30 p.p.m. could be due to $Si(N_3C)$ sites, and a chemical shift around -20 p.p.m. could be the precise location for the SiC bond. The ^{13}C solid state NMR data are shown in Fig. 9. Only one resonance peak was observed at 13.7 ppm. This is probably due to an SiC bond according to the established data [16–18].

An important feature for the ^{29}Si NMR data is that all the resonance peaks are rather broad. This effect could be due to the amorphous nature of the samples and the presence of silicon oxynitride bonds. Well-crystallized Si_3N_4 would have a chemical shift at -46.6 p.p.m. for α-type Si_3N_4 [19] and -48.9 p.p.m. for β-type Si_3N_4 [17], and silicon oxynitride would have a chemical shift around 55 p.p.m. The chemical shifts for the samples analysed here, however were -43.9 and -43.9 p.p.m. rather than -46.4 or -48.9 p.p.m.

It should be noted that no graphite carbon was evident in the ^{13}C spectrum, but was observed in the C(1s) spectra of the XPS studies. Therefore, it was concluded that the obtained ceramic powder exhibited a rich nanostructure with the presence of complex phases. The majority phases included silicon nitride (Si_3N_4), nonstoichiometric silicon nitride (Si_xN_y), silicon carbide (SiC), and small quantities of silicon oxycarbonitride or $SiC_aO_bN_c$ in tetrahedral structures [21], as well as a trace amount of SiO_2.

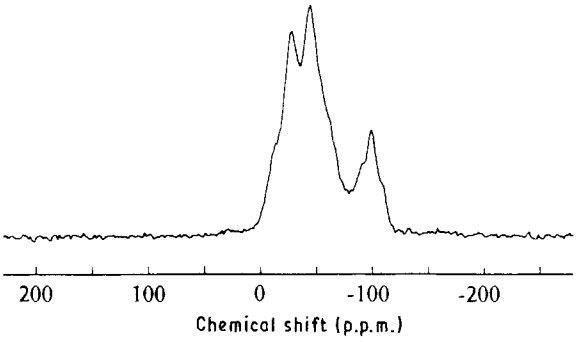

Figure 8 ^{29}Si MAS-NMR of the ultrafine ceramic particles derived from pyrolysis of the silazane precursor.

4. Proposed model

The silazane precursor was rapidly evaporated into molecular vapour. The precursor vapour then reacted with NH_3 to form Si_3N_4 and SiC ceramic products at high temperature, presumably according to

$$[CH_3SiHNH]_{3 \text{ or } 4} \xrightarrow{NH_3} Si_3N_4 + SiC + \text{by-products} \quad (1)$$

A theoretical analysis of the thermal conversion of liquid monomer to ceramic nanoparticles has to consider (i) the high driving force for this rapid process, which is created by the large temperature difference between the hot reaction zone inside the furnace and the cooled collector, and (ii) the mechanisms of the particle formation by rapid condensation. Because no visible particle deposition was observed at the hot furnace region it is assumed the hot vapours are rapidly cooled, and condensed on the cooled collector as they emerge from the reaction zone. In this process, the host gas and the vapour species are assumed to

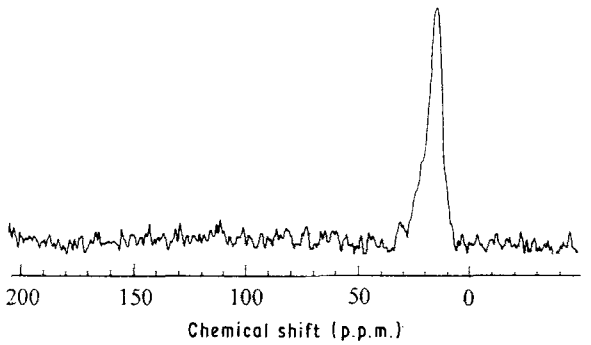

Figure 9 ^{13}C MAS-NMR of the ultrafine ceramic particles derived from pyrolysis of the silazane precursor.

move with a velocity v_f

$$v_f = \frac{F_{gas} + F_{vapour} + F_{volatile}}{\pi r^2} \quad (2)$$

Here F_{gas} is the flow rate of the host gas or NH_3, F_{vapour} the flow rate of the vapour species derived from the precursor flow rate, $F_{volatile}$ the volatile species from the reacted precursor, and r the radius of the reaction tube, 1.4 cm.

In Equation 1, the by-products are assumed to be volatile gases including $4H_2$ and $3CH_4$. The NH_3 gas flow rate was measured to be 2.5 $cm^3 s^{-1}$ which corresponds to 1.12×10^{-4} $mol\,s^{-1}$. The liquid precursor flow rate was measured to be 9×10^{-3} $cm^3 s^{-1}$, which corresponds to 0.3×10^{-4} $mol\,s^{-1}$. Thus the molar ratio of NH_3 to $(CH_3SiHNH)_4$ is in the ratio of 3:1. At a temperature of 1273 K, it is assumed that a $(CH_3SiHNH)_4$ molecule in the vapour phase will rapidly convert to one Si_3N_4, one SiC, four CH_4, and eight H_2 molecules. Thus the molar concentration for NH_3:Si_3N_4:SiC:CH_4:H_2 would be 3:1:1:3:4. The estimated partial pressures would be 0.58 atm for these volatile species, 0.25 atm for NH_3 and 0.17 atm for ceramic vapours. Knowing the gas flow rate and the precursor flow rate and the partial pressures for each species, the flow rate, F, at that temperature for gas, vapour and volatile species can be estimated using the ideal gas law. They are calculated to be F_{gas} = 40.3 $cm^3 S^{-1}$, $F_{volatile}$ = 94.0 $cm^3 s^{-1}$, and F_{vapour} = 26.8 $cm^3 s^{-1}$. Therefore, V_f is estimated to be 26.2 $cm\,s^{-1}$. The cooling rate can be defined as

$$\frac{dT}{dt} = \frac{dT}{dl} v_f \quad (3)$$

where $dT/dl \simeq \Delta T/r$, with T = 1273 K, v_f = 26.2 $cm\,s^{-1}$, the cooling rate is calculated to be 1.87×10^4 $K\,s^{-1}$, and the cooling time is 5.35×10^{-2} s.

During the time t, the cooling time, each molecule sweeps out a volume $\sigma_c vt$, where σ_c is the cross-section of a molecule. The molecules which condense are contained in a volume of $(Dt)^{3/2}$, where D is the diffusivity, v is the root mean square molecular speed. Thus, the probability that any molecule hits the nucleus is

$$P = \frac{\sigma_c vt}{(Dt)^{3/2}} \quad (4)$$

Again, it is assumed that particle growth does not begin until the gas leaves the hot furnace and neglects the fact that the monomer concentration decreases as the particle growth proceeds. Assuming there are N $mol.cm^{-3}$ for ceramic vapour, each molecule has a volume of a^3, in the diffusion accessible volume $(Dt)^{3/2}$, the upper limit for the number of molecules that will condense (N_{cond}) surrounding the nucleus would be

$$N_{cond.} = \frac{\sigma_c vt}{(Dt)^{3/2}} N(Dt)^{3/2}$$

$$= \sigma_c vtN \quad (5)$$

The upper limit volume of the condensate becomes

$$V = \sigma_c vtNa^3 \quad (6)$$

Here the cross-section σ_c is assumed to be 8×10^{-16} cm^2, a is assumed to be 4×10^{-8} cm, and v is estimated to be 1.1×10^5 $cm\,s^{-1}$. N can be estimated to be 9.8×10^{17} $mol\,cm^{-3}$ using the ideal gas law and Avogadro's number. Therefore, the volume of a condensed particle is determined to be 2.95×10^{-16} cm^3, which corresponds to a diameter of 82.6 nm.

Microstructural analysis has indicated that the smallest condensate diameter is about $\sim$ 20 nm, and the largest condensate has a diameter of about $\sim$ 150 nm. As revealed by transmission electron microscopy, the larger diameter particles appear to form by smaller particle coalescence. Critical factors in the theoretical overestimate of the condensed particle diameter (by a factor of 4) are the assumptions: (i) unity sticking coefficient, and (ii) constant monomer concentration. Clearly, in practice, these values might be reduced significantly. Analysis of these factors continues in the development of the present model.

5. Conclusion

Recent investigation has demonstrated the possibility of synthesizing nanoscale ceramic powders by thermal reactor conversion of organosilazane liquid precursor using an aerosol injection method. The process can be carried out at atmospheric pressure. A particle-size prediction model gives results in agreement with the experimental observations. This work emphasizes the merits of a synergistic approach involving organometallic/polymer chemistry and material processing. Current studies are focused on the elimination of oxygen contamination from the pyrolysis environment.

Acknowledgement

The authors thank the University of Connecticut Research Foundation for partial financial support of this research. Particular thanks are also due to Professor Alan Jones, Professor Paul Inglefield and Mr Changan Zhang, Clark University, for the NMR analysis.

References

1. R. BIRRINGER and H. GLEITER, "Encyclopedia of Materials Science and Engineering", Supp. Vol. 1, edited by R. W. Cahn (Pergamon Press, Oxford, 1988) p. 339.
2. J. EASTMAN and R. SEIGEL, *Res. Devel.* January (1989) 56.
3. T. D. XIAO, P. R. STRUTT and K. E. GONSALVES, *Mater. Res. Soc. Symp.* **168** (1990) 199.
4. K. E. GONSALVES, P. R. STRUTT and T. D. XIAO, *Adv. Mater.* (1991) 202.
5. K. E. GONSALVES, P. R. STRUTT, T. D. XIAO and P. G. KLEMENS, *J. Mater. Sci.* **27** (1992) 3231.
6. D. SEYFERTH, G. H. WISEMAN and C. PRUDHOME, *J. Amer. Ceram. Soc.* **66**, (1983) c13.
7. D. SEYFERTH and G. H. WISEMAN, *ibid.* **67**, (1984) c132.
8. J. P. PARTRIDGE and P. R. STRUTT, *SPIE* **669** (1986) 150.
9. C. L. BEATY in "Ultrastructure Processing of Advanced Structural and Electronic Materials" edited by L. L. Hench (Noyes Data, New Jersey), (1984) 256.
10. J. WONG and C. A. ANGELL, "Glass Structure by Spectroscopy" (Marcel Dekker, New York, 1976) p. 547.
11. M. J. RAND and J. F. ROBERTS, J. Electrochem. Soc. **120** (1973) 446.
12. S. T. RAIDER, R. FLISTCH, J. A. ABOAF and W. A. PLISKIN, *ibid.* **123** (1976) 560.
13. R. KARCHER, L. LEY and R. L. JOHNSON, *Phys. Rev. B* **30** (1984) 1890.
14. E. BOUILLON, O. MOCAER, J. F. VILLENEUVE, R. PAILLER, R. NASLAIN, M. MONTHIOUX, A. OBERLIN, C. GUIMON and G. PFISTER, *J. Mater. Sci.* **26** (1991) 1517.
15. Y. XIE and P. M. A. SCHERWOOD, *Chem. Mater.* **1** (1989) 427.
16. G. D. SORARU, FLORENCE, BONNEAU and T. D. MACKENZIE, *J. Mater, Sci.* **25** (1990) 3886.
17. R. M. STEWART, N. R. DANDO, D. SEYFERTH and A. J. PERROTTA, *Amer. Chem. Soc. Symp.* **32** (3) (1991) 569.
18. F. BABONNEAU, J. LIVAGE and R. M. LAINE, *ibid.* **32** (3) (1991) 579.
19. K. R. CARDUNER, R. O. CARTER III, M. E. MILBERG and M. CROSBIE, *Anal. Chem.* **59** (1987) 2794.
20. K. R. CARDUNER, R. O. CARTER III, M. J. ROKOSZ, C. PETERS, G. M. CROSBIE and E. D. STILES, *Chem. Mater.* **1** (1989) 302.
21. J. LIPOWITZ, *Ceram. Bull.* **70** (1991) 1888.

Received 12 February 1992
and accepted 16 June 1992